Theory and experiment of a 94 GHz gyrotron traveling-wave amplifier[a)]

H. H. Song,[1] D. B. McDermott,[1] Y. Hirata,[1] L. R. Barnett,[2] C. W. Domier,[1] H. L. Hsu,[1] T. H. Chang,[2] W. C. Tsai,[2] K. R. Chu,[2] and N. C. Luhmann, Jr.[1,b)]
[1]*Department of Applied Science, University of California, Davis, California 95616*
[2]*Department of Physics, National Tsing Hua University, Hsinchu, Taiwan, Republic of China*

(Received 27 October 2003; accepted 4 February 2004; published online 23 April 2004)

Experimental results are presented on the first W-band gyrotron Traveling-Wave Tube (gyro-TWT) developed to exploit the 94 GHz atmospheric window for long-range, high-resolution radar applications. The gyro-TWT is designed to operate in the higher order TE_{01} mode and is driven by a 100 kV, 5 A electron beam with a pitch angle of $v_\perp/v_z=1$ and velocity spread of $\Delta v_z/v_z=5\%$. Large-signal simulations predict 140 kW output power at 92 GHz with 28% efficiency, 50 dB saturated gain, and 5% bandwidth. The stability of the amplifier against spurious oscillations has been checked with linear codes. To suppress the potential gyro-BWO interactions involving the TE_{02}, TE_{11}, and TE_{21} modes, the interaction circuit with a cutoff frequency of 91 GHz has been loaded with loss so that the single-path, cold-circuit attenuation is 90 dB at 93 GHz. A coaxial input coupler with 3% bandwidth is employed with a predicted and measured coupling of 1 dB and 2 dB, respectively. The operating voltage is limited to below 75 kV because of oscillations encountered at higher voltages in this initial embodiment. Preliminary test at $V_b=60$ kV and $I_b=3.7$ A yielded 59 kW saturated output power at 92.2 GHz with 42 dB gain, 26.6% efficiency, and a 3 dB bandwidth of 1.2 GHz (1.3%). © *2004 American Institute of Physics.* [DOI: 10.1063/1.169064]

I. INTRODUCTION

High power millimeter wave gyrotron amplifiers are of considerable interest for advanced radar applications including remote sensing, precision tracking, imaging, and jet engine modulation (JEM) classification.[1–4] Based on the cyclotron maser instability, gyrotron amplifiers lend themselves to the use of overmoded interaction circuits that allow efficient production of high peak and average power operations at millimeter wavelengths.

In particular, the gyrotron traveling wave amplifier (gyro-TWT), in which an electromagnetic wave is amplified at the harmonic of the electron cyclotron frequency has long been viewed as an extremely promising device due to the potential for broadband operation while retaining the high efficiency and high gain features associated with gyrotron devices. Despite this promise, the early performance of gyro-TWT's proved to be severely limited due to oscillations caused by various instabilities[5–7] which resulted in a decade long hiatus in gyro-TWT research. However, in a recent round of theoretical and experimental studies by the National Tsing Hua University (NTHU), Taiwan, high output power and gain have been achieved in Ka-band gyro-TWT's by increasing circuit loss to suppress numerous oscillations. A TE_{11} mode ultrahigh gain gyro-TWT with 93 kW power, 70 dB saturated gain, 26.5% efficiency with 3 dB bandwidth of 8.6% has been demonstrated at NTHU, with distributed wall loss configuration.[8,9] Using this approach at the Naval Research Laboratory (NRL), a TE_{11} mode gyro-TWT experiment with distributed loss scheme produced 78 kW power, 60 dB saturated gain, 19% efficiency with 3 dB bandwidth of 17.1%.[10,11] Also at NRL, a lossy ceramic loaded TE_{01} gyro-TWT achieved 137 kW power, 47 dB saturated gain, 17% efficiency with 3 dB bandwidth of 3.3%.[12]

In radar applications, the millimeter wave portion of the spectrum, especially the 94 GHz window at W-band offers superior performance through clouds, fog, and smoke. This need has led to interest in the development of W-band gyrotron amplifiers. An early 94 GHz, gyro-TWT at Varian produced 20 kW power, 30 dB saturated gain, 8% efficiency with a 3 dB bandwidth of 2%.[2] Recently, Communications and Power Industries (CPI) has demonstrated a W-band gyrotwystron which produced 60 kW power, 34 dB saturated gain, 15% efficiency with 3 dB bandwidth of 1.6 GHz.[13,14] Also at CPI, a gyroklystron operating in the TE_{01} mode has achieved 100 kW power, 35 dB saturated gain, and 30% efficiency with 3 dB bandwidth of 0.7 GHz and has been employed in NRL's W-band Advanced Radar for Low Observable Control (WARLOC) system.[13,14]

Despite the success of previous W-band gyroamplifier demonstrations, there still remains a critical challenge for an amplifier with considerably wider bandwidth to support the use of appropriately chirped pulses with pulse compression for high resolution radar operations. To satisfy this need, a wide bandwidth W-band gyro-TWT technology development effort has been carried out at the University of California, Davis. In this paper, design and results of experimental demonstration are presented for a high performance 94 GHz TE_{01} gyro-TWT amplifier with a distributed wall loss configuration, a technique recently employed in NTHU's Ka-band ultrahigh gain gyro-TWT experiment.[8,9] The design and theo-

[a)]Paper LI2 5, Bull. Am. Phys. Soc. **48**, 201 (2003).
[b)]Invited speaker.

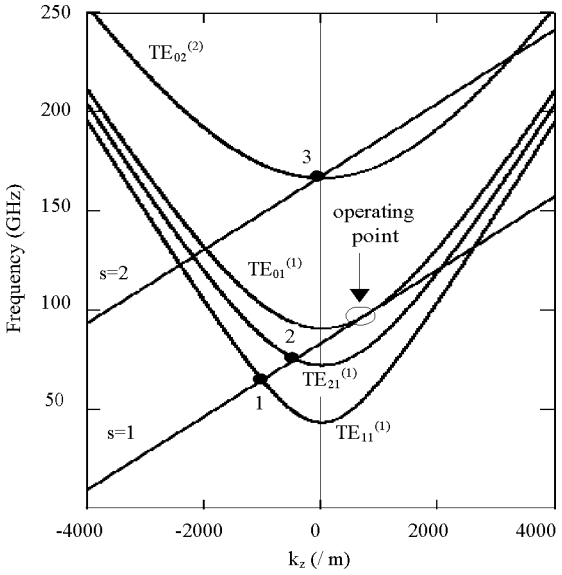

FIG. 1. Dispersion diagram of the fundamental TE_{01} gyro-TWT interaction with possible oscillation modes for $V_b=100$ kV and $v_\perp/v_z=1.0$.

retical predictions are described in Sec. II. The experimental setup, together with the results and discussion are presented in Sec. III. In Sec. IV, summary and future directions are discussed.

II. DESIGN AND THEORETICAL PREDICTIONS

The dispersion diagram of the fundamental TE_{01} gyro-TWT interaction is shown in Fig. 1 for the design beam voltage of $V_b=100$ kV and velocity ratio of $v_\perp/v_z=1.0$. For higher efficiency, the magnetic field is chosen so that the fundamental cyclotron resonance nearly grazes the TE_{01} operating mode ($B_0/B_g=0.995$). It is well known that interactions at the backward wave region where the fundamental or second harmonic cyclotron resonance lines intersect with a waveguide mode (point 1, 2, and 3 in Fig. 1) are potential sources of absolute instabilities.[15–17] To suppress potential competing mode oscillations at the second harmonic TE_{02}, the fundamental harmonic TE_{11}, and the fundamental harmonic TE_{21} modes, the first 12 cm of the 14.5 cm long circuit has been loaded with lossy carbon colloid with a resistivity of $70\,000\rho_{Cu}$, where ρ_{Cu} is the resistivity of copper ($\rho_{Cu}=1.72\times10^{-6}$ Ω cm).[18] Stability codes have been employed to determine the required loss. The application method and modeling of lossy layers are described in detail in Ref. 18. The measured insertion loss of the TE_{01} gyro-TWT circuit was 90 dB at 93 GHz.

The performance of the TE_{01} gyro-TWT has been evaluated using a self-consistent nonlinear particle-tracing code[8] to meet the power, bandwidth, gain, and efficiency requirements. The nonlinear interaction models are used to perform parametric studies of circuit parameters, beam parameters, magnetic field, wall losses, and structural nonuniformities. The loaded and unloaded length of the circuit was determined using small-signal codes to ensure stable operation. For the design parameters (Table I), 140 kW saturated output power with 28% efficiency, 5% bandwidth, and 50 dB saturated gain were predicted for a velocity spread of $\Delta v_z/v_z=5\%$, as shown in Fig. 2. It has been shown analytically,[19] wall losses of the amplifier absorbs electromagnetic energy of the reflected waves three times more than that of the amplified signal and has little effect in efficiency.

TABLE I. Design parameters of the heavily loaded TE_{01} gyro-TWT amplifier.

Voltage	100 kV
Current	5 A
$\alpha=v_\perp/v_z$	1.0
$\Delta v_z/v_z$	5%
Magnetic field, B_0	35.6 kG
B_0/B_g	0.995
Cutoff frequency	91.0 GHz
Lossy wall resistivity	$70\,000\,\rho_{Cu}$
Guiding center radius, r_c	$0.45\,r_w$
Circuit radius, r_w	0.201 cm
Lossy circuit length	11.0 cm
Loss taper length	1.0 cm
Copper circuit length	2.5 cm
Total circuit length	14.5 cm

The TE_{01} input and output couplers have been designed using the Agilent High Frequency Structure Simulator (HFSS) code. As shown in Fig. 3, the TE_{10} fundamental mode in the rectangular waveguide couples to the coaxial cavity in TE_{51} mode and then through the five slots spaced equally 72° azimuthally, the TE_{51} mode couples to the operating TE_{01} mode. An input coupler with ~1 dB insertion loss and 3% bandwidth was employed in the experiment presented in this paper. A wider bandwidth (7%) input coupler has been designed and fabricated for the next stage of the experiment. Figure 4 shows the comparison between HFSS simulation and the cold test measurement of this optimized input coupler. To monitor the output power, an output coupler with ~10 dB coupling was employed. The output coupler shares the same geometry as the input coupler but the coupling is reduced to ~10 dB by adjusting the slot and coaxial cavity parameters and thus eliminated the possibility

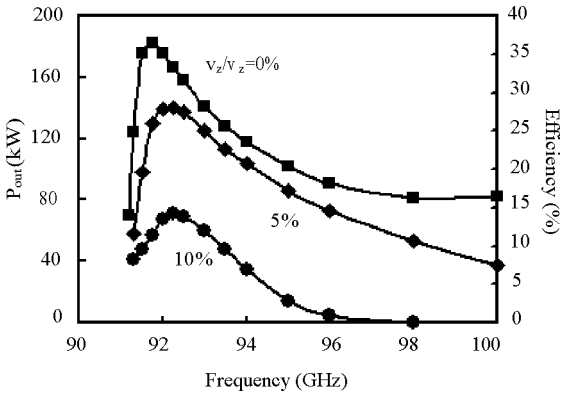

FIG. 2. Predicted performance of the TE_{01} gyro-TWT for velocity spread of $\Delta v_z/v_z=0\%$, 5%, and 10%. Other parameters are given in Table I.

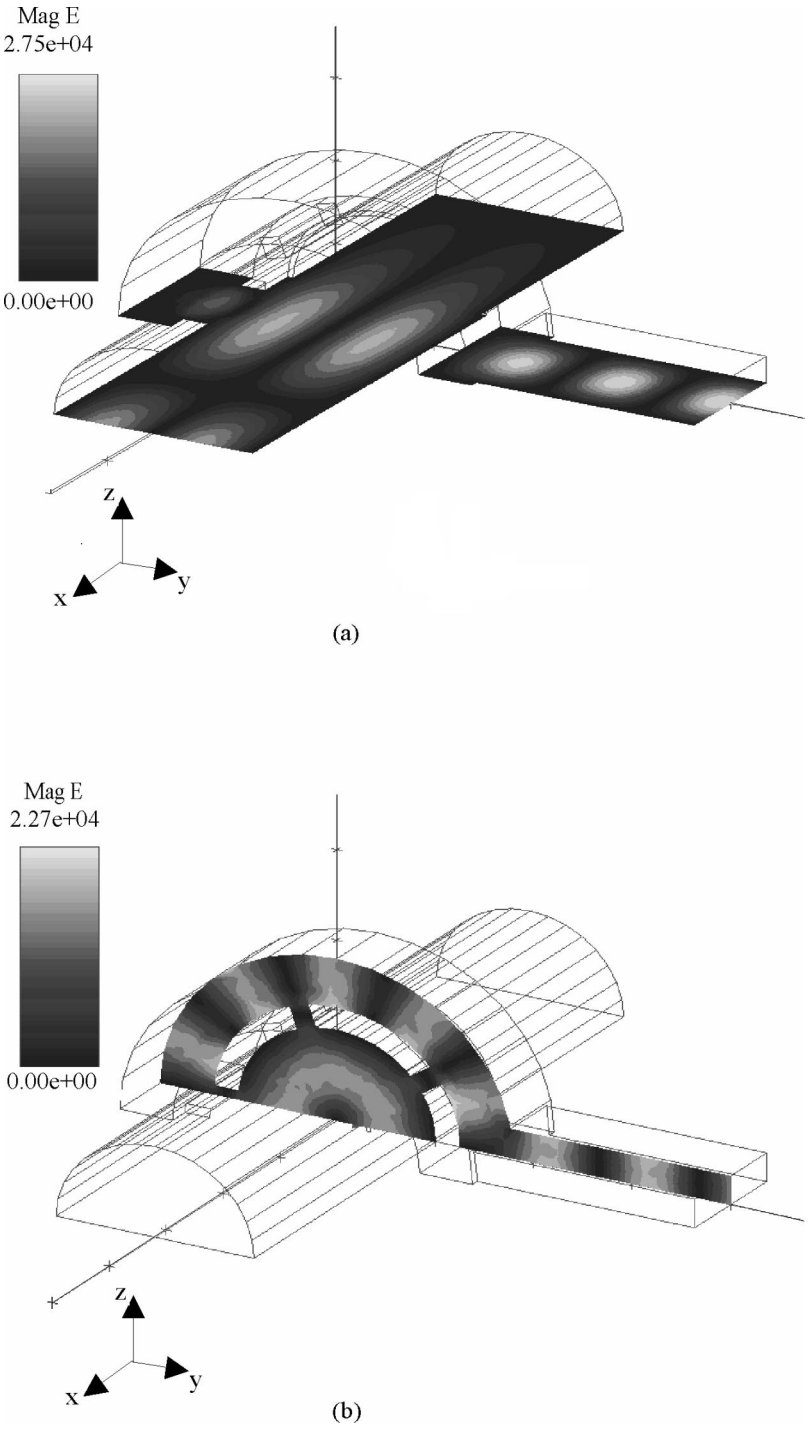

FIG. 3. HFSS simulation results showing intensity of electromagnetic fields in the TE_{01} input coupler (a) axial view and (b) cross-sectional view.

of waveguide breakdown problems. The output coupler exhibits greater than ~10 dB coupling over a 5% bandwidth.

To achieve the desired velocity spread for the design velocity ratio, beam voltage, and current, a single anode Magnetron Injection Gun (MIG) was initially designed using the variable mesh FINELGUN code[20] and has been later optimized using the EGUN code. Figure 5 shows electron trajectories, equipotential lines, and the magnetic field profile for $V_b = 100$ kV and $I_b = 5$ A from EGUN simulation. The predicted velocity spread was $\Delta v_z / v_z = 2.2\%$ for the design velocity ratio of $v_\perp / v_z = 1.0$. The fabricated MIG employs a Scandate cathode assembly manufactured by Spectramat and the edges of the emitting strip have been coated with molybdenum to suppress edge emission. The MIG employed in this experiment is a modification of the NTHU MIG design.[21]

III. EXPERIMENTAL SETUP, RESULTS, AND DISCUSSION

A. Experimental setup

The schematic of the integrated TE_{01} gyro-TWT system is shown in Fig. 6. The experimental setup consists of rf input and output couplers, MIG electron gun, interaction circuit, superconducting magnet, high voltage modulator, input

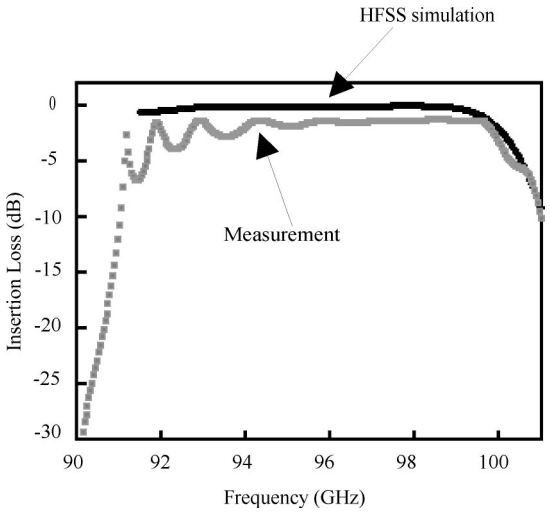

FIG. 4. A comparison of the HFSS simulation and cold test measurement results of the optimized broadband TE_{01} input coupler.

driver and rf diagnostics. The magnetic field is generated by a 50 kG refrigerated superconducting magnet system. The uniformity of the axial magnetic field is $\pm 0.1\%$ over 50 cm, as stipulated in the design specification and verified by measurements with a Hall probe. The solenoid is comprised of four independent compensated coils. Two trim coils in the gun region were used to adjust the velocity ratio of the MIG beam and produce nearly zero field in the interaction region. The main interaction coils produce nearly zero field in the gun region and contain both solenoidal and gradient coils. To produce the desired magnetic field amplitude and gradient at the emitter of the electron gun, the emitter has been positioned at the null of the gun gradient coil. Using this arrangement, both the amplitude and the gradient of the axial magnetic field at the cathode can be independently adjusted. The magnetic field at the cathode emitter was nominally 1 kG and as the gyrating beam enters the interaction region it is adiabatically compressed by a typical operating main magnetic field of 35 kG. The axial alignment of the circuit was provided by four sets of micrometers held at both ends of the circuit for optimum transmission and circuit performance. An electrically isolated current collector is placed after the output coupler to effectively monitor beam transmission through the circuit. A Rogowski loop measured both emitted

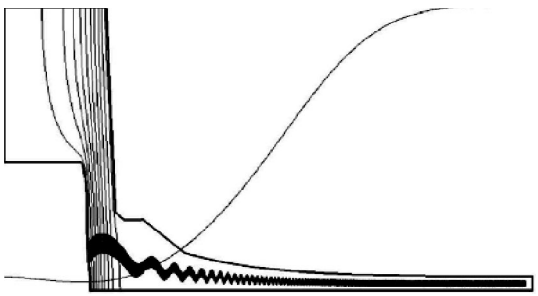

FIG. 5. Magnetron Injection Gun (MIG) simulation results from EGUN code showing electron trajectory, equipotential lines, and magnetic field profile. $\Delta v_z/v_z = 2.2\%$ velocity spread predicted for velocity ratio of $v_\perp/v_z = 1.0$ and beam voltage of $V_b = 100$ kV.

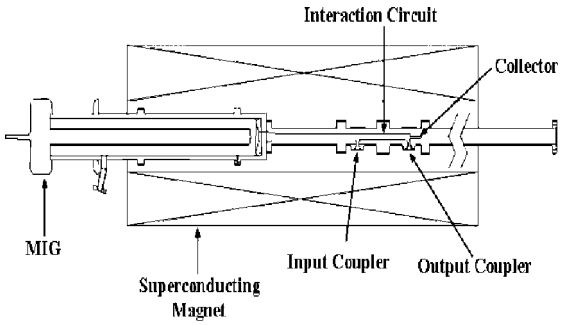

FIG. 6. Schematic of the TE_{01} gyro-TWT amplifier.

and collected current. A Macor load coated with carbon colloid material was placed between output coupler and the collector to absorb 90% of the rf power since only 10% of the generated power couples through the output coupler.

The rf drive signal was provided by a 100 W, 5% bandwidth Hughes folded waveguide continuous wave TWT. To shield the driver from the high magnetic field of the gyro-TWT, the output of the driver was connected to the input coupler of the gyro-TWT through a 10 foot long Ka-Band overmoded waveguide run. The input driver was pulsed to produce a 1 μs duration signal with a repetition rate of 1–2 Hz. A remotely controlled HP synthesized sweeper drives the folded waveguide TWT and determines the input frequency. The rf diagnostics are designed such that the rf input power, output power, and the oscillation power can be monitored separately through a waveguide switch, directional coupler, precision variable attenuator and crystal detector. The output power and input drive power was varied using a precision variable attenuator and a frequency meter was used to identify the frequency of the amplified output signal. In addition, to identify possible competing modes (TE_{02} mode at 167 GHz, TE_{11} mode at 66 GHz, and the TE_{21} mode at 75 GHz), a Fabry–Perot interferometer has been employed. This interferometer is comprised of two mesh plates, two horn antennas, a crystal detector, and a moving stage with micrometer attached. By measuring the distance between the adjacent detected signal peaks, the frequency of the signal was determined. All the components were calibrated using an Agilent 8510C W-band vector network analyzer and precision power meters.

B. Experimental results and discussion

Based on the design and theoretical predictions previously described, the experiment was designed with parameters specified in Table I. However, in this initial embodiment, optimum performance was found to occur for reduced beam voltages (60–70 kV) due to various oscillations encountered at higher beam voltages as discussed in the following. During the experiment, the TE_{01} gyro-TWT system was optimized to yield maximum performance at 92.2 GHz where highest power and gain are predicted and measurements were made at other frequencies under the same beam voltage, beam current, and magnetic field operating conditions. The temporal history of beam voltage, collected beam current, rf input and output typical pulse traces from a diode

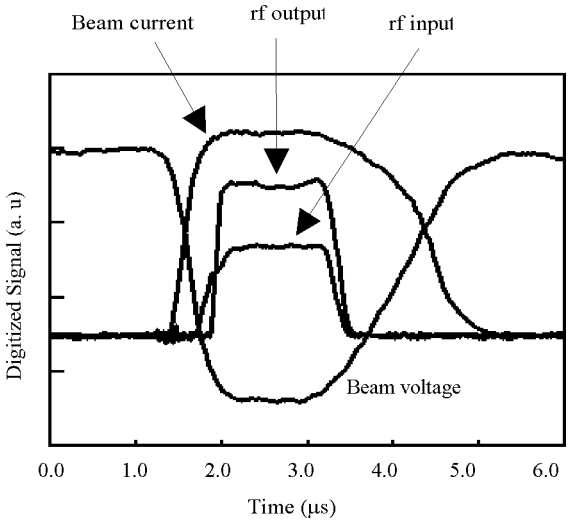

FIG. 7. Temporal history of beam voltage, collected beam current, rf input and output traces.

detector is shown in Fig. 7. To maintain the synchronism between beam voltage pulse and rf input drive pulse, an adjustable delay generator has been used.

The dependence of typical output power on input power for several frequencies are shown in Fig. 8 for $V_b = 56$ kV, $I_b = 3.7$ A, and $B_0 = 34.1$ kG. As the input power increases output power linearly grows until it reached saturation at an input power level of ~ 5 W. Further increase in input power results in energy recovery of electrons from rf and the amplifier becomes overdriven. The measured transfer property indicates good linearity at low beam voltages for stable operation.

The saturated drive bandwidth of the amplifier after retuning for optimum operating parameters is displayed in Fig. 9 for $V_b = 60$ kV, $I_b = 3.7$ A, and $B_0 = 34.0$ kG. For this operating condition, the amplifier exhibited 59 kW saturated output power at 92.2 GHz with 42 dB gain, 26.6% efficiency, and 3 dB bandwidth of 1.2 GHz (1.3%). The relatively narrow bandwidth is believed to be attributed to beam degradation at the drift region resulting in higher than predicted velocity spread in the system. A more detailed discussion follows at the end of this section. It must be noted that the cutoff of the TE_{01} gyro-TWT circuit is 91 GHz and that there may be limitations due to the current 3% input coupler where at 97 GHz, the insertion loss becomes very large. With the improved bandwidth input coupler of 7%, which will be employed in the next stage of the experiment, the current limitations can be removed. The better matched output coupler near cutoff frequency of 91 GHz, will contribute to the broader bandwidth operation. The design and optimization of the new output coupler is underway.

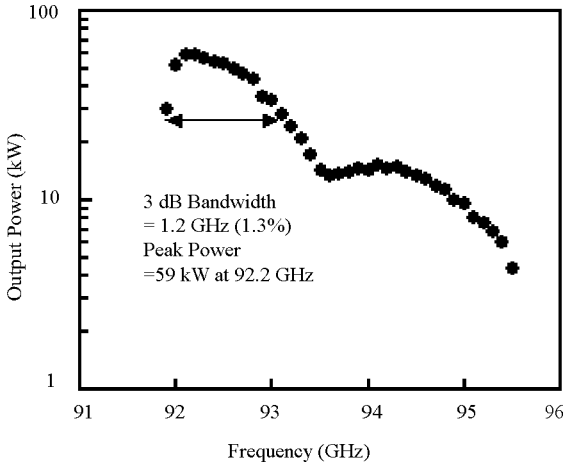

FIG. 9. Measured saturated output power versus the frequency for $V_b = 60$ kV, $I_b = 3.7$ A, and $B_0 = 34.0$ kG.

Stability studies have been performed at various conditions with and without input drive power present. By using waveguide switches, the amplified signal and the oscillation signal were monitored simultaneously using crystal detectors. As shown in Fig. 10, the second harmonic TE_{02} mode has been predicted as the most probable competing mode. Figure 11 shows the measured amplified TE_{01} output power and the TE_{02} oscillation power versus input power for $V_b = 70$ kV, $I_b = 5.3$ A, and $B_0 = 34.3$ kG. The oscillation frequency has been measured at 170 GHz using Fabry–Perot

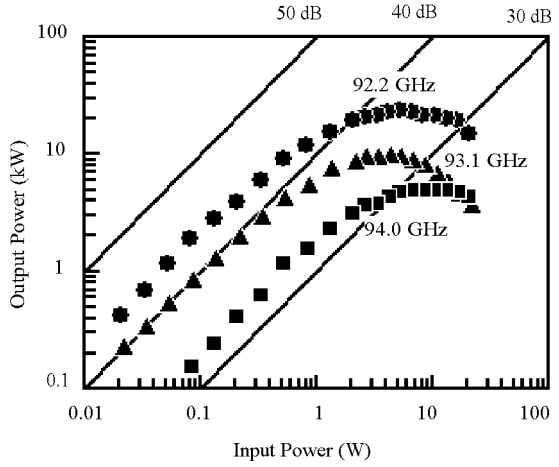

FIG. 8. Measured output power versus the drive power for $V_b = 56$ kV, $I_b = 3.7$ A, and $B_0 = 34.1$ kG for drive frequencies of 92.2, 93.1, and 94.0 GHz.

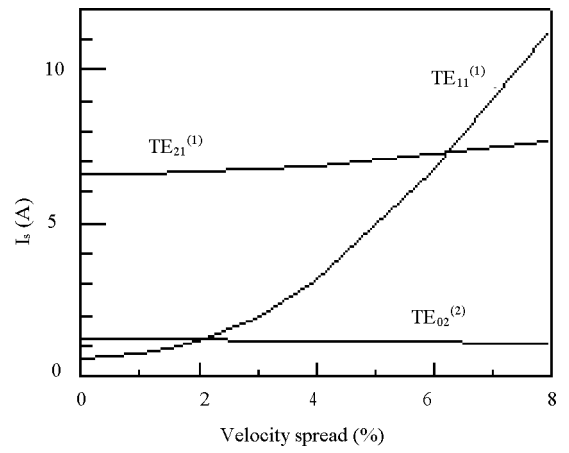

FIG. 10. Calculated start oscillation currents of the most likely competing mode as functions of velocity spread.

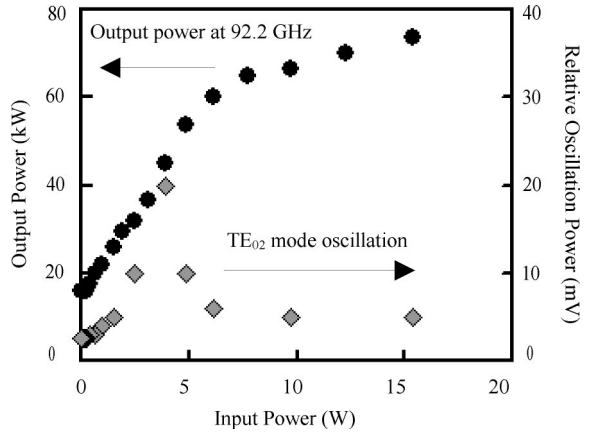

FIG. 11. Measured output power at 92.2 GHz and competing TE_{02} mode relative oscillation power at 170 GHz versus input power for $V_b=70$ kV, $I_b=5.3$ A, and $B_0=34.3$ kG.

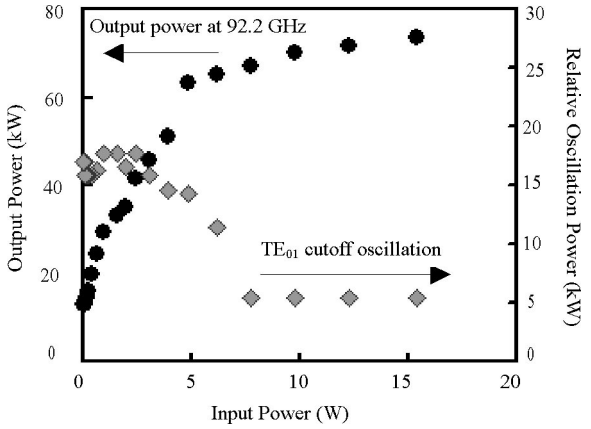

FIG. 13. Measured output power at 92.2 GHz and TE_{01} relative oscillation power at ~91 GHz versus input power for $V_b=72$ kV, $I_b=5.3$ A, and $B_0=34.1$ kG.

interferometer and identified as the second harmonic TE_{02} mode. The oscillation power was measured using waveguide cutoff sections to reject the amplified signal at W-band and so that only the TE_{02} mode was monitored. Note that the bump increase in amplified signal coincides with the rapid decrease in oscillation power. This feature indicates clear evidence of mode competition and suppression in the TE_{01} gyro-TWT, similar to the competition and suppression of the TE_{21} oscillation in the TE_{11} gyro-TWT reported in Ref. 7. The dependence of oscillation power on beam voltage is indicated in Fig. 12. Similarly, the rapid drop in gain coincides with the rapid jump in oscillation power above ~73 kV. Another type of oscillation observed was the absolute instability of the TE_{01} mode near the cutoff frequency of 91 GHz. Figures 13 and 14 shows the dependence of output power and cutoff oscillation power on input driver power. This indicates that the TE_{01} absolute instability can also be partially suppressed with increasing drive power. The cutoff oscillation power was measured using tunable cavity filter that has been designed to pass only the desired frequency. Different from the competing mode oscillations in the gyro-TWT circuit, oscillations were observed in the drift region of the tube just next to the input coupler. Using the Fabry–Perot interferometer, the oscillation frequency was measured at ~85 GHz and identified as the TE_{01} mode. After analysis of the suspected oscillation region, it was discovered that a design oversight had resulted in the cyclotron resonance line intersecting with the TE_{01} waveguide mode at ~82 GHz in the input drift section. Consequently, even though this region was heavily loaded, it is believed that this led to beam quality degradation and is attributed to the observed narrow bandwidth. The change in the radius of the drift region due to finite thickness of the carbon colloid loading can be responsible for the difference in the measured frequency.

IV. SUMMARY

The results of a W-band heavily loaded TE_{01} gyro-TWT amplifier development was described. In this initial embodiment, optimum performance occurred for reduced beam voltages (60–70 kV) due to various oscillations encountered at higher voltages. The amplifier exhibited 59 kW saturated output power at 92.2 GHz with 42 dB gain, 26.6% efficiency, and 3 dB bandwidth of 1.2 GHz (1.3%) with a $V_b=60$ kV, $I_b=3.7$ A MIG electron beam. Three types of oscillations were observed: TE_{02} competing mode oscillation at 170

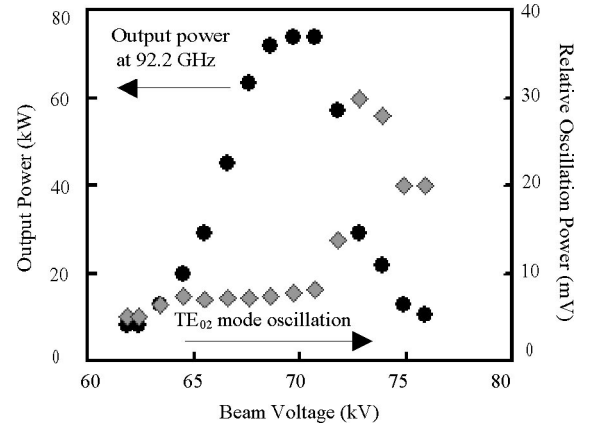

FIG. 12. Measured output power at 92.2 GHz and TE_{02} relative oscillation power at 170 GHz versus beam voltage for $I_b=5.4$ A and $B_0=34.3$ kG.

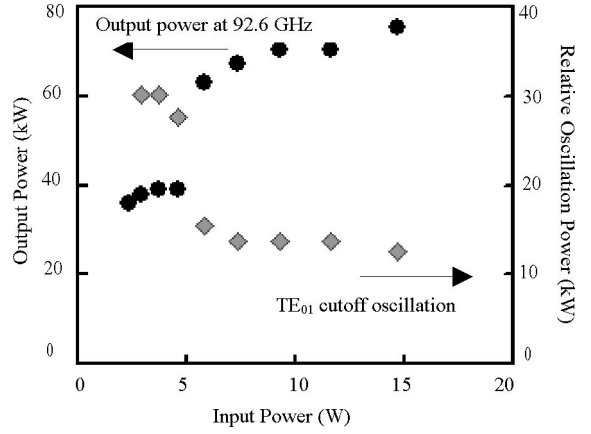

FIG. 14. Measured output power at 92.6 GHz and TE_{01} relative oscillation power at ~91 GHz versus input power for $V_b=80$ kV, $I_b=5.1$ A, and $B_0=34.8$ kG.

GHz, TE_{01} mode cutoff oscillation near 91 GHz, and drift tube oscillation at ~85 GHz. In order to suppress the unwanted oscillations, a modified interaction section with shorter unloaded length and a drift tube with smoothly tapered structure will be employed in the next experimental version. The shorter unloaded interaction section has been predicted to increase the threshold current for the competing mode oscillation and therefore will lead to a stable operation. The performance for the modified interaction circuit has been evaluated with a self-consistent nonlinear particle tracing code. Also, an improved bandwidth input coupler of 7% and better-matched output coupler at the cutoff frequency of 91 GHz will be used to enhance the performance of the tube.

ACKNOWLEDGMENTS

The assistance of P. Marandos, J. Lee, M. Johnson, and L. Dressman is gratefully acknowledged.

This work has been supported by AFOSR under Grants No. F49620-99-1-0297 (MURI MVE) and No. F49620-00-1-0339.

[1]W. M. Manheimer, G. Mesyats, and M. I. Petelin, in *Applications of High-Power Microwaves*, edited by A. V. Gaponov-Grekhov and V. L. Granatstein (Artech House, Boston, 1994), pp. 169–207.
[2]V. L. Granatstein, B. Levush, B. G. Danly, and R. K. Parker, IEEE Trans. Plasma Sci. **25**, 1322 (1997).
[3]K. L. Felch, B. G. Danly, H. R. Jory, K. E. Kreischer, W. Lawson, B. Levush, and R. J. Temkin, Proc. IEEE **87**, 752 (1999).
[4]W. M. Manheimer, A. W. Fliflet, K. St. Germain, G. J. Linde, W. J. Cheung, V. Gregers-Hansen, B. G. Danly, and M. T. Ngo, Geophys. Res. Lett. **30**, 1103 (2003).
[5]L. R. Barnett, K. R. Chu, J. M. Baird, V. L. Granatstein, and A. T. Drobot, *Technical Digest International Electron Devices Meeting* (IEEE, New York, 1979), pp. 164–167.
[6]L. R. Barnett, J. M. Baird, Y. Y. Lau, K. R. Chu, and V. L. Granatstein, *Technical Digest International Electron Devices Meeting* (IEEE, New York, 1980), pp. 314–317.
[7]L. R. Barnett, L. H. Chang, H. Y. Chen, K. R. Chu, W. K. Lau, and C. C. Tu, Phys. Rev. Lett. **63**, 1062 (1989).
[8]K. R. Chu, H. Y. Chen, C. L. Hung, T. H. Chang, L. R. Barnett, S. H. Chen, T. T. Yang, and D. J. Dialetis, IEEE Trans. Plasma Sci. **27**, 391 (1999).
[9]K. R. Chu, H. Y. Chen, C. L. Hung, T. H. Chang, L. R. Barnett, S. H. Chen, and T. T. Yang, Phys. Rev. Lett. **81**, 4760 (1998).
[10]K. T. Nguyen, J. P. Calame, D. E. Pershing, B. G. Danly, M. Garven, B. Levush, and T. M. Antonsen, IEEE Trans. Plasma Sci. **48**, 108 (2001).
[11]D. E. Pershing, J. P. Calame, K. T. Nguyen, B. G. Danly, and B. Levush, *Proceedings of the 2nd International Vacuum Electronics Conference* (Noordwijk, The Netherlands, 2001), p. 145.
[12]M. Garven, J. P. Calame, B. G. Danly, K. T. Nguyen, B. Levush, F. N. Wood, and D. E. Pershing, IEEE Trans. Plasma Sci. **30**, 885 (2002).
[13]M. Blank, B. G. Danly, B. Levush *et al.*, Phys. Plasmas **6**, 4405 (1999).
[14]M. Blank, K. Felch, B. G. James *et al.*, IEEE Trans. Plasma Sci. **30**, 865 (2002).
[15]Y. Y. Lau, K. R. Chu, L. R. Barnett, and V. L. Granatstein, Int. J. Infrared Millim. Waves **2**, 373 (1981).
[16]A. T. Lin, K. R. Chu, and A. Bromborsky, IEEE Trans. Electron Devices **34**, 2621 (1987).
[17]K. R. Chu and A. T. Lin, IEEE Trans. Plasma Sci. **16**, 90 (1988).
[18]D. B. McDermott, H. H. Song, Y. Hirata *et al.*, IEEE Trans. Plasma Sci. **30**, 894 (2002).
[19]Y. Y. Lau, K. R. Chu, L. Barnett, and V. L. Granatstein, Int. J. Infrared Millim. Waves **2**, 395 (1981).
[20]M. Caplan and C. Thorington, Int. J. Electron. **51**, 415 (1981).
[21]Ch. Wang, Y. S. Yeh, T. T. Yang, H. Y. Chen, S. H. Chen, Y. C. Tsai, L. R. Barnett, and K. R. Chu, Rev. Sci. Instrum. **68**, 3031 (1997).